

Document downloaded from:

<http://hdl.handle.net/10251/149720>

This paper must be cited as:

Bellido-Millán, P.J.; Lera, R.; Seimetz, M.; Ruiz-De La Cruz, A.; Torres Peiró, S.; Galán, M.; Mur, P.... (2017). Characterization of protons accelerated from a 3 TW table-top laser system. *Journal of Instrumentation*. 12:1-12. <https://doi.org/10.1088/1748-0221/12/05/T05001>



The final publication is available at

<https://doi.org/10.1088/1748-0221/12/05/T05001>

Copyright IOP Publishing

Additional Information

Characterization of protons accelerated from a 3 TW table-top laser system

P. Bellido,^{a,b,c,1} R. Lera,^{b,1} M. Seimetz,^{a,2} A. Ruiz-de la Cruz,^b S. Torres-Peirò,^b M. Galán,^b P. Mur,^a I. Sánchez,^b R. Zaffino,^d L. Vidal,^a A. Soriano,^a S. Sánchez,^a F. Sánchez,^a M.J. Rodríguez-Álvarez,^a J.P. Rigla,^a L. Moliner,^a A. Iborra,^a L. Hernández,^a D. Grau-Ruiz,^a A.J. González,^a J.J. García-Garrigos,^a E. Díaz-Caballero,^a P. Conde,^a A. Aguilar,^a L. Roso,^c J.M. Benlloch^a

^a*Instituto de Instrumentación para Imagen Molecular (I3M),
Camino de Vera s/n, Ed. 8B-N-1^a, 46022 Valencia, Spain*

^b*Proton Laser Applications S.L. (PLA),
Av. Vilafranca del Penedès 11A, 08734 Olèrdola (Barcelona), Spain*

^c*Centro de Láseres Pulsados (CLPU),
C/ Adaja 8, 37185 Villamayor (Salamanca), Spain*

^d*Instituto de Microelectrónica de Barcelona (IMB-CNM, CSIC),
C/ dels Til.lers Campus UAB, 08193 Cerdanyola del Vallès (Barcelona), Spain*

E-mail: mseimetz@i3m.upv.es

ABSTRACT: We report on benchmark tests of a 3 TW/50 fs, table-top laser system specifically developed for proton acceleration with an intrinsic pump rate up to 100 Hz. In two series of single-shot measurements differing in pulse energy and contrast the successful operation of the diode pumped laser is demonstrated. Protons have been accelerated up to 1.6 MeV in interactions of laser pulses focused on aluminium and mylar foils between 0.8 and 25 μm thickness. Their spectral distributions and maximum energies are consistent with former experiments under similar conditions. These results show the suitability of our system and provide a reference for studies of laser targets at high repetition rate and possible applications.

KEYWORDS: Accelerator applications, lasers, plasma generation (laser-produced)

¹This work comprises part of the results of the Ph.D. theses of P. Bellido and R. Lera.

²Corresponding author.

Contents

1	Introduction	1
2	Experimental setup	2
2.1	Laser system	2
2.2	Particle detectors	4
3	Experimental results	6
4	Conclusions and outlook	9

1 Introduction

The acceleration of protons and ions to multi-MeV energies by highly intense lasers has become a very active research field [1, 2]. Experiments at dedicated laser facilities cover a broad range of parameters, including the laser pulse energy (of the order 0.1-100 J), peak power (1-1000 TW), and pulse duration (femtoseconds to picoseconds). First applications of this technique which, due to the very high field gradients achieved in laser-plasma interactions, potentially constitutes a compact source of accelerated particles, are envisaged or have already been demonstrated, especially in medicine [3] and radiobiology [4, 5]. Nevertheless, the realisation of a complete, laser-based setup delivering proton beams of controlled energy (or well-known spectral distribution) and (pulsed) intensity remains a technical challenge. It typically comprises a high-power, femtosecond laser with intrinsically high repetition rate, suitable targets which have to be renewed and precisely positioned at the laser focus, and particle detectors for the spectral characterisation of the protons. Several optical parameters strongly affect the particle spectra, such as the pulse energy on target, laser spot size, and pulse contrast. In order to assess the reliability of the laser operation benchmark tests can be performed and compared to well-known results.

Systematic studies of laser-proton acceleration under a wide range of conditions have been performed using plain foil targets. These typically consist of metal [6–11] or mylar foils [12–15] with thicknesses between some tens of nanometers to tens of micrometers which are individually placed at the focussed laser spot. Some authors applied reels or wheels with continuous foils for multiple laser shots [16–18]. The influence of single optical parameters has been investigated such as the variation of the maximum proton energy with the laser prepulse duration [19] or the pulse contrast [20]. In addition, the foil thickness has been varied over a wide range [19, 21, 22]. Interestingly, despite numerous differences between these experiments common features have been revealed such as the Boltzmann-like form of continuous proton spectra, interpreted in the framework of Target Normal Sheath Acceleration (TNSA) [23], and general trends have been observed relating, for example, the maximum proton energy with the laser power or the laser pulse energy on target

(see discussion in section 4). This broad data base can therefore be used to evaluate the performance of a new experimental setup over a wide range of intrinsic parameters.

In this communication we report on the first, systematic characterisation of laser-accelerated protons from a novel table-top, high repetition rate system developed specifically by one of the partner institutions. In the present configuration its pulsed power is of 2-3 TW on the laser target at 10-100 Hz pump rate. Continuous proton spectra have been obtained in two experimental series differing in pulse energy and contrast with aluminium and mylar targets between 0.8 and 25 μm thickness. While improvements on other components of our experimental setup, especially the laser target, will be necessary to fully exploit its high-rate capability, the present study shows that this compact, modular device is an adequate tool for the investigation of laser-ion acceleration and for the development of future applications of this technique.

2 Experimental setup

2.1 Laser system

Our experiments have been performed with a table-top laser reaching a maximum pulsed power of 3 TW (165 mJ pulse energy behind the compressor in 55 fs)¹. Two independent series have been run differing in several optical parameters (see Table 1). Following the chirped-pulse amplification scheme [24], the initial pulses (10 fs, 6 nJ) of a titanium-sapphire (Ti:Sa) oscillator² are stretched to about 100 ps and then amplified in three stages. First, the beam passes a regenerative oscillator that provides pulses of 1.5 mJ. In a second step, two multi-pass Ti:Sa stages amplify the pulses up to the final energy of 150 mJ (265 mJ) in series 1 (2), respectively. Each amplifier is pumped independently at 100 Hz (10 Hz), respectively, by a frequency-doubled Nd:YLF laser (527 nm). It is possible to operate the laser in single shot mode or up to 100 Hz repetition rate. A train of small prepulses originating from the regenerative amplifier, 10-100 ns ahead of the main pulse, have been observed in the first tests. Their suppression by careful synchronisation of the Pockels cells of the regenerative amplifier has proven to be crucial for the efficient acceleration of protons. In series 1 the remaining prepulse level has been of the order 10^{-2} - 10^{-3} . Two saturable absorbers of 2 mm thickness have been implemented in series 2 only, one behind the regenerative amplifier and one behind the first multipass amplifier. They allow for further reduction of the intensity of spurious prepulses down to 10^{-5} - 10^{-6} with respect to the main peak [25] as measured with a photodiode. The ASE pedestal level has been estimated to be of the order 10^{-8} in this configuration.

In series 1 and 2 the pulse is compressed on a pair of gratings to 43 fs (55 fs) duration FWHM, respectively, as measured with a self-referenced spectral interferometry system [26] (Figure 1). The compressed pulse contains 93 mJ (165 mJ), respectively, representing a maximum power of 2 TW (3 TW) centred at 800 nm wavelength.

The compressed laser pulses are guided into the interaction chamber. Two primary pumps maintain a pressure level around 10^{-2} mbar in the vacuum system, which is sufficient to avoid laser filamentation in air and to guarantee negligible energy loss of the accelerated protons before reaching the detectors. The focusing system consists of a 60° , $f/3$ gold protected off-axis parabolic mirror

¹Proton Laser Applications S.L., Olèrdola (Spain).

²Venteon, Laser Quantum.

Table 1. Optical parameters in two series of experiments. The most important difference concerning proton acceleration is the increased contrast of series 2.

	Series 1	Series 2
Pulse energy (pre-compression)	150 mJ	265 mJ
Pulse energy behind comp.	93 mJ	165 mJ
Pulse duration (FWHM)	43 fs	55 fs
Peak power	2 TW	3 TW
Focal spot (FWHM, μm^2)	5.0×9.0	5.0×11.5
Peak intensity (10^{18} W/cm^2)	3.7	4.0
Prepulse level	10^{-2} - 10^{-3}	10^{-5} - 10^{-6}
ASE level	$\sim 10^{-5}$	$\sim 10^{-8}$
Pump rate	100 Hz	10 Hz

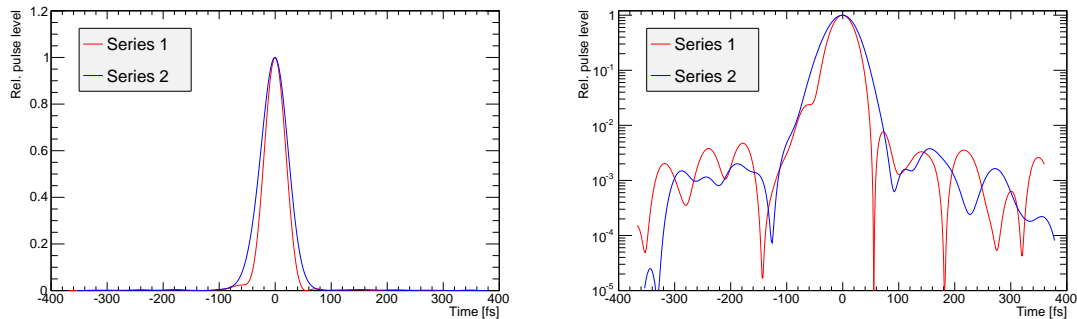


Figure 1. (Color on-line) Temporal pulse structure on the femtosecond scale for the two laser configurations.

(OAP). The size of the focal spot is about $5 \times 10 \mu\text{m}^2$ FWHM. It has been directly measured using a CCD camera and an aspheric lens with $0.57 \mu\text{m}$ effective pixel size. The complete experimental setup downstream of the laser amplifiers is depicted in Figure 2.

The target holder, designed for single-shot operation with individual target alignment, is mounted on a three-axis platform that allows for positioning of the target with a precision better than $2.5 \mu\text{m}$. Laser pulses are focused onto thin foils at an incidence angle of 30° to avoid back reflection and to prevent damage of the particle detectors. A collimated, 632 nm He:Ne laser beam is guided into the Ti:Sa beam path for control of the target position in transverse direction. In addition, light reflected from the target is recollectored on a screen and visualized by a CCD camera outside the vacuum chamber. Provided a typical surface roughness of the target material on the scale of the laser wavelength, an interference pattern (“speckle”) is formed which varies with the size of the irradiated area [27] and thus with the longitudinal distance of the target from the laser focus. The optimum position is identified by visual inspection of the reflection pattern. The precision of this method has been estimated to about $25 \mu\text{m}$ in longitudinal direction with a Rayleigh length of $70 \mu\text{m}$, corresponding to an uncertainty around 12% in the peak intensity. Improvements, such as an automatic pattern analysis and alignment, and alternative methods like direct visualization by a microscope and CCD camera are presently under study.

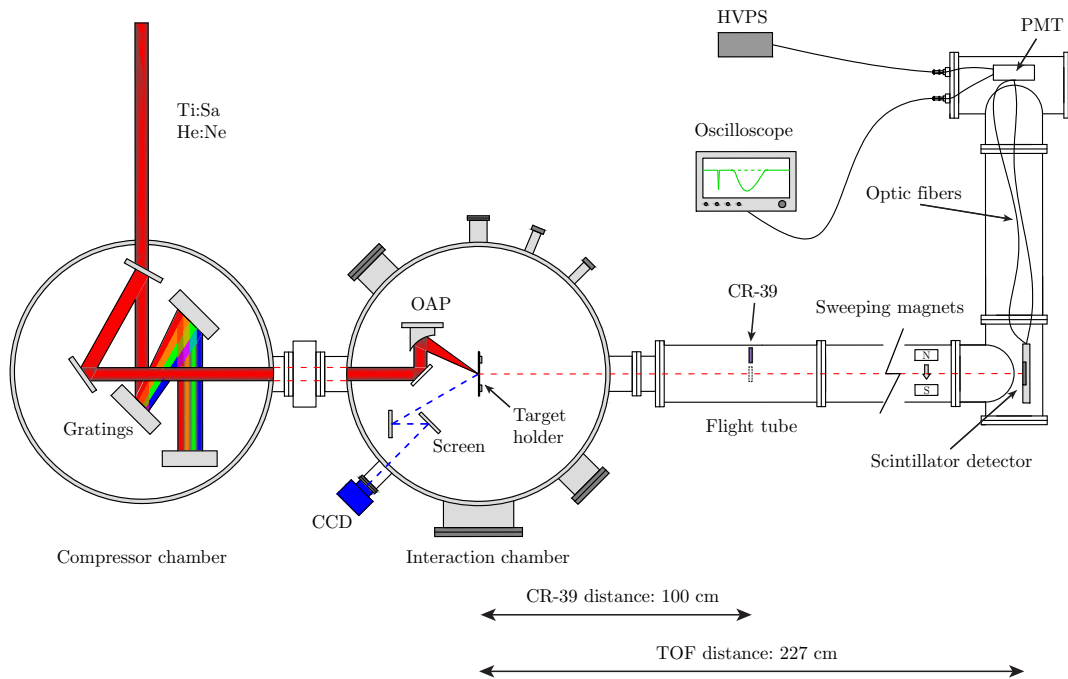


Figure 2. (Color on-line) Schematic view of the interaction chamber and particle detectors.

2.2 Particle detectors

In the present study, two complementary methods have been applied for the detection of protons and the measurement of their energies. CR-39 nuclear track detectors have been used in all experiments. The main advantages of this passive material are its high specificity to protons and ions and its sensitivity to single particles. In addition, we have exploited a relation between track diameters and proton energies. For this purpose, a calibration has been performed with proton beams of 0.1-5.5 MeV from a 3 MV tandem accelerator (National Accelerator Centre (CNA), Seville). For CR-39 plates etched with 6.25M NaOH at 90°C during 4 hours, the track diameters increase monotonically for proton energies below 1 MeV. Up to this limit the proton spectra can therefore be directly obtained from the track size distribution. To this purpose, the plates have been scanned with an automatic microscope (Radosys PT10³) and track diameters have been measured with a ROOT-based code developed by the authors. In this analysis, the pixel size of the images is of 0.6 μm , which is sufficient for a precise discrimination of the observed track diameters ($\leq 30 \mu\text{m}$). The CR-39 plates of 1 cm² area were placed 100 cm behind the laser target. Part of them were covered with aluminium foils of 4 or 7 μm thickness, respectively, to absorb the lowest energy protons and to extend the dynamic range beyond 1 MeV. The controlled energy loss of protons exceeding the respective thresholds of 400 and 600 keV has been utilised to calculate their initial energies.

For the measurements at higher laser power (series 2) an online monitor has been implemented in our setup, consisting in a plastic scintillator coupled to a photomultiplier (PMT). Its dynamic range can be adjusted by neutral density filters reducing the number of scintillation photons reaching

³Radosys, Budapest (Hungary), www.radosys.com

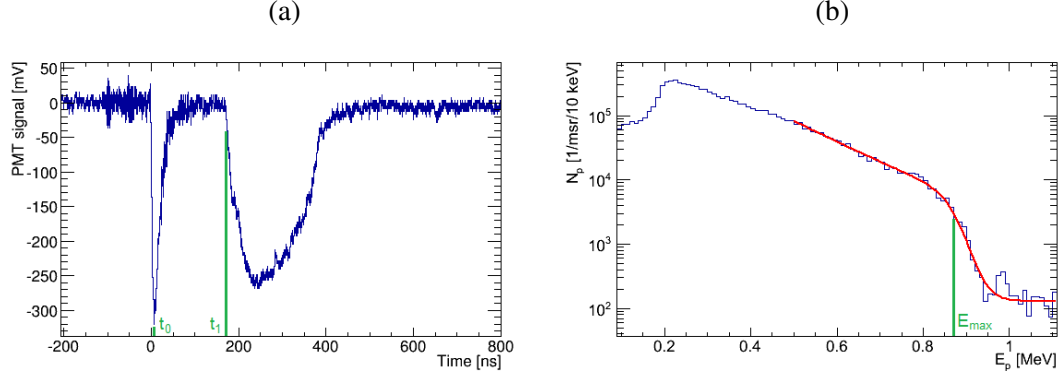


Figure 3. (Color on-line) (a) Time-of-flight signal from a laser shot on a 7 μm thick Al target foil, recorded on a scintillator with 0.04 msr angular acceptance at $d = 227$ cm in normal direction behind the target. The most energetic protons arrive at time t_1 . (b) Proton spectrum calculated from TOF with fitted function, Eq. (3.1), and maximum energy, E_{max} .

the PMT. In previous calibrations with pulsed proton beams from a 3 MV tandem accelerator [28] we have established relations between the output signal height, U , recorded on a fast oscilloscope, and the number of protons in a 100 ns long time interval, N_{100} , which may be written as

$$N_{100}(U) = \frac{U}{m - \alpha U}. \quad (2.1)$$

Here, $m = 5.24 \cdot 10^{-3}$ mV and $\alpha = 5.212 \cdot 10^{-6}$ are calibration factors corresponding to the present configuration. This detector allows for determination of the proton kinetic energy by the time-of-flight technique [10] and the measurement of absolute spectral distributions as follows. In the PMT anode signals two peaks can clearly be distinguished (Figure 3(a)). The leading edge of the first one, originating from photons and relativistic electrons, has been used as trigger signal, while the second peak corresponds to protons (low-energetic electrons are swept away by a dipole magnet with 0.04 Tm field integral in front of the scintillator). For each bin of width $\Delta t = 0.2$ ns of the timing spectra the proton kinetic energy, E_p^i , is calculated from the measured time after the photon peak taking into account the delay of the start signal at $d = 227$ cm target distance. The number of particles in bin i is obtained from the signal height, U_i , following eq. (2.1),

$$N_i(E_p^i) = N_{100}(U_i) \cdot \frac{\Delta t}{100 \text{ ns}} \cdot \frac{1}{\Omega E_p^i}. \quad (2.2)$$

The factor $1/E_p^i$ accounts for the fact that protons up to 22.5 MeV are stopped in the scintillator and the PMT signal height is approximately proportional to their kinetic energy. Ω is the solid angle covered by the detector through a circular collimator ($\Omega = 0.04$ msr). Finally, the N_i are summed up in a histogram of equally sized energy bins, Figure 3(b). The maximum proton energy, E_{max} , corresponds to the leading edge of the second peak in Figure 3(a). In part of the measurements, CR-39 and the online monitor have been applied simulatenously; the resulting maximum energies coincide within 100 keV.

3 Experimental results

A systematic comparison of proton energies obtained from aluminium and mylar target foils with different thicknesses has been performed for the two series of laser parameters specified above. All reported results are from single shot experiments with individual target alignment. In series 1 (93 mJ pulse energy behind the compressor) major numbers of proton tracks have been observed on CR-39 plates for aluminium foils between 7 and 25 μm (Figure 4). They differ strongly in track density and diameters.

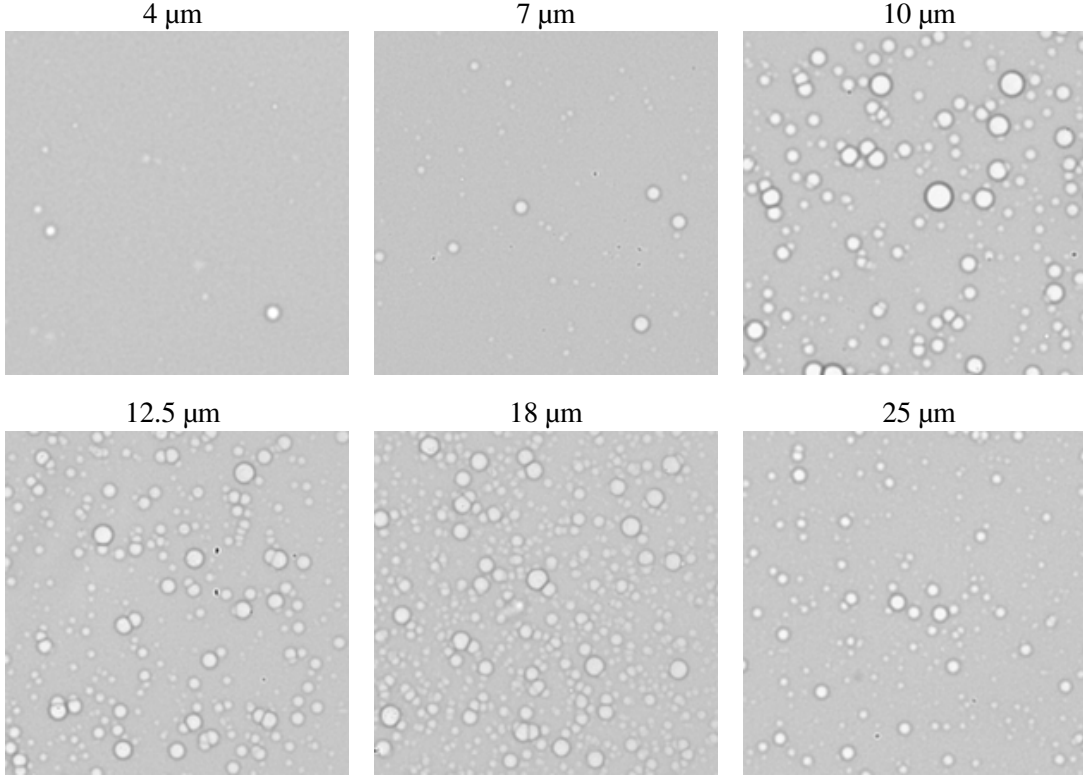


Figure 4. Images of CR-39 plates showing proton tracks from Al foil targets of various thicknesses. Differences in track density and diameters are apparent. Proton spectra extracted from the track size distributions are presented in Figure 5.

A series of microscopic images have been analysed for each chip in order to obtain the spectral distributions shown in Figure 5. The number of protons, N_p , as a function of proton energy, E_p , can be approximated analytically by

$$N_p = \frac{N_0}{E_p} \cdot e^{-E_p/k_B T} / (1 + e^{(E_p - E_{\max})/\Delta E}) + N_{bg}. \quad (3.1)$$

This spectral form comprises a Boltzmann distribution [29] with a mean ion temperature, T , and a parameter for the particle number at low energies, N_0 . The term in parentheses accounts for the observed high-energy cutoff, E_{\max} , over a short interval, ΔE (this width has been found between 14 and 25 keV for all data sets of Figure 5). In this series, the maximum proton energies were below 1 MeV. Particle numbers close to the maximum were of the order $10^4/\text{msr}$ while the integral over

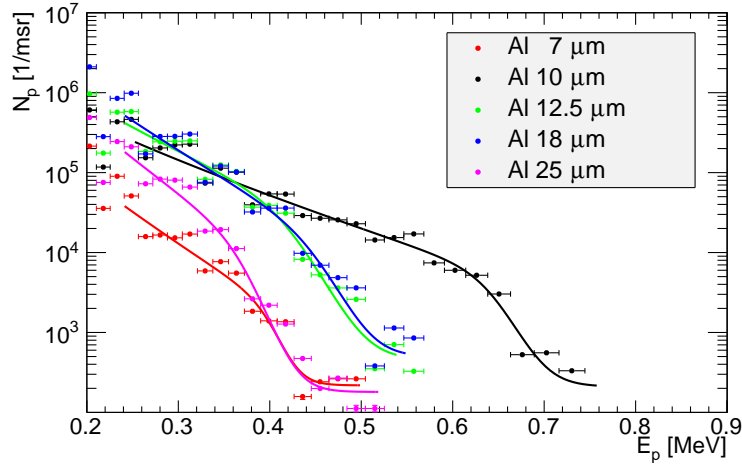


Figure 5. (Color on-line) Spectral distribution of laser-accelerated protons from Al target foils of different thickness (series 1, low contrast), measured with CR-39 plates.

the entire spectral range was two orders of magnitude higher. The constant background, N_{bg} , was added to improve the fit quality. It was found to be at least 1000 times smaller than the leading factor, N_0 . Under the conditions of series 1 and with thinner aluminium foils (below 7 μm) as well as mylar foils (6 and 13 μm thickness), no significant track numbers have been observed as compared to the background level on the CR-39 plates.

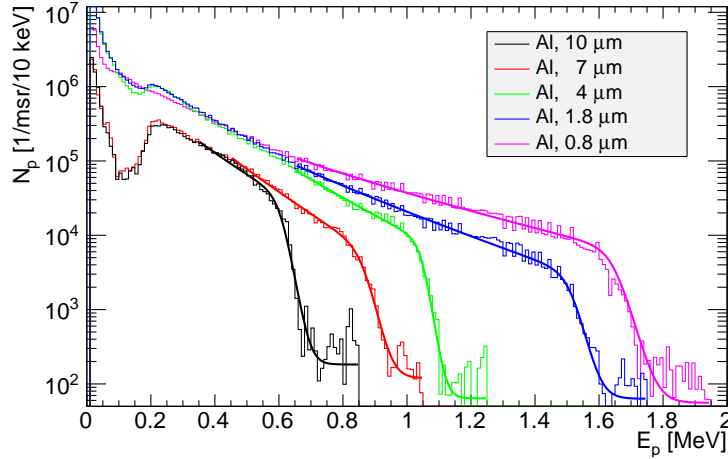


Figure 6. (Color on-line) Spectral distribution of laser-accelerated protons from single shots on Al target foils of different thickness (series 2, high contrast), measured with the TOF detector.

In series 2 (265 mJ), protons have been observed for a much wider range of target sizes (0.8-18 μm for aluminium). The energy spectra calculated from the time-of-flight signals have been fitted with the same analytic function, Eq. (3.1), as those derived from track diameters on CR-39. Examples of single-shot spectra are shown in Figure 6. For convenience, these histograms are plotted up to the limit of the fitted intervals. In addition, proton acceleration from mylar foils has

been demonstrated. Pure mylar of 6 and 13 μm has been used while the 2 μm thick foil was covered with a thin aluminium coating on the laser impact side. The maximum proton energies are compared in Figure 7, showing the mean value and standard deviation for several (typically 4-5) laser shots on the same target material. For comparison, the results of series 1 are included as well. For thick Al foils (10 μm or more) the proton energies obtained in series 1 and 2 are very similar. Below this value major differences can be observed. At 7 μm , E_{max} is more than twice as high with 265 mJ laser pulses as compared to 150 mJ. At even thinner targets, where no significant track numbers have been observed in series 1, proton energies up to 1.6 MeV have been measured in series 2. An increase towards thinner targets can clearly be seen in Figure 7. Similar particle energies have been observed with mylar foils from which we did not obtain clear proton tracks in series 1.

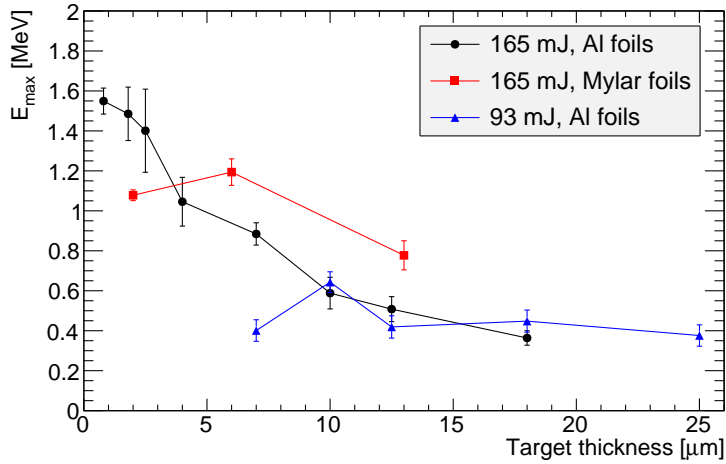


Figure 7. (Color on-line) Maximum proton energies from Al and mylar target foils of different thickness for two series with 165 mJ and 93 mJ laser energy behind the compressor, respectively.

As indicated in Table 1, two main changes have been made between settings 1 and 2, increasing both the laser pulse energy and contrast. In order to test the relevance of contrast on the acceleration of protons, an additional series of measurements were done removing the saturable absorber in front of the first multipass amplifier. This resulted in an increase in energy to 300 mJ (pre-compression) and a decrease in contrast (not better than 10^{-5} for the prepulse level). However, protons accelerated in this experiment, using targets of different thicknesses, did not reach energies beyond 1 MeV. We interpret our results in the way that the improved contrast (up to three orders of magnitude) was more decisive for the increase in particle energy than the gain in pulse energy or peak intensity (less than a factor 2). This is qualitatively similar to the findings by Ceccotti and coworkers [20] who presented a direct comparison between low and high contrast results. They also observed an optimum foil thickness (20 μm) for limited contrast, with absence of protons at 3 μm or less, while at high contrast E_{max} continuously increased towards sub-micron targets.

In Figure 8(a) we compare the maximum proton energies obtained in series 1 and 2 to those of other, published experiments with femtosecond laser pulses below 3 J incident on plain foil targets. Only the highest proton energies of each publication are shown, together with their respective target material and thickness (in μm). Data have been divided into two groups with moderate contrast

ratio (up to 10^7) [7–10, 13, 14, 16–18, 20, 30, 31] and high contrast ($\geq 10^8$) [11, 15, 19–21, 32–35], respectively. In our series 1, the maximum proton energy has been achieved with a 10 μm thick aluminium foil while no acceleration has been observed with 4 μm or less. Other experiments at moderate contrast used target thicknesses between 2.5 and 23 μm . A $E_p = k \cdot E_L^{1/2}$ tendency, indicated by the blue, dotted line, seems to be a fair approximation to the general trend of this data set (here, $k = 2$ in units of $\text{MeV}/\text{J}^{1/2}$). At high contrast, much thinner foils have often given better results, similar to our series 2 at 0.8 μm (red line, $k = 6$). Note that the same square root dependency with $k = 4$ was proposed in [1] to describe all data points over a much larger energy interval. A recent comparison of data including experiments on ultra-thin foils as well as low-density and microstructured targets suggests a steeper rise ($E_p \propto E_L$) [36, 37].

Simplified models of laser-plasma interactions typically relate the maximum proton energy to the laser power, P_L , rather than the pulse energy [19, 38]. Zeil *et al.* [34] propose a formalism which has been applied in Figure 8(b) as follows. Data have been selected according to the laser pulse duration; we restrict our discussion to an interval around 45 fs corresponding to our experiment. These data have been divided according to the target thickness, d . The continuous line represents the model calculations for 43 fs laser pulses incident on a 10 μm thick target foil within a spot of 2.5 μm radius, corresponding to our series 1. The dashed line is for 55 fs pulses and $d = 0.8 \mu\text{m}$. Our data point of series 2 is close to the latter one, and the area delimited by both lines may be understood as an indication of the general evolution with these laser parameters. Both figures show that the proton energies observed in our experiments are consistent with previous results.

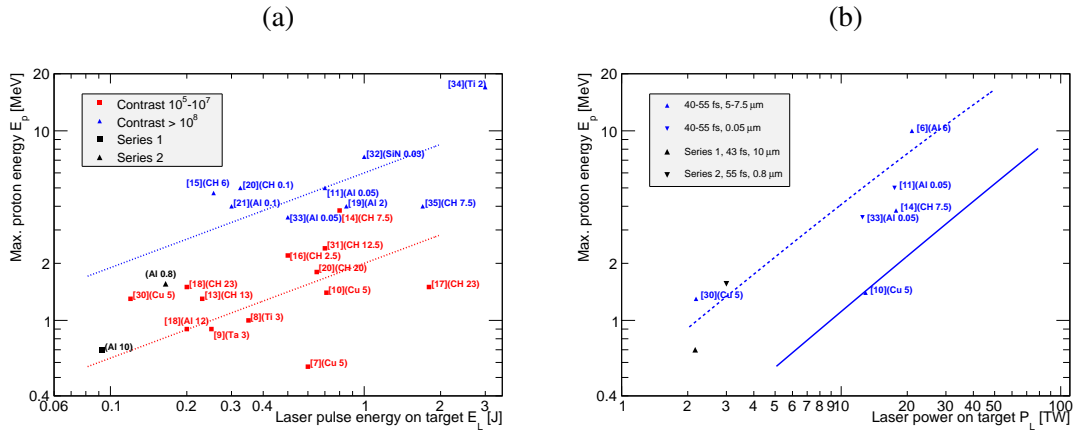


Figure 8. (Color on-line) (a) Maximum proton energies as a function of laser energy on target from published experiments and our series 1 and 2. Labels indicate the material and thickness of target foils; CH refers to organic compounds. (b) Maximum proton energies as a function of laser power. Here, only data with 40-55 fs pulse duration have been chosen. The lines show calculations based on the model presented by Zeil *et al.* [34].

4 Conclusions and outlook

We report on the first demonstration of proton acceleration up to 1.6 MeV with a novel table-top laser system developed by the authors. A laser power of 2-3 TW has been focused on thin foil targets

of various thicknesses, achieving peak intensities up to 4.0×10^{18} W/cm². The measured particle energies correspond to those expected from other, published results at similar laser parameters. An improvement in prepulse contrast from $\sim 10^{-3}$ to $\sim 10^{-6}$ has been crucial for the use of target foils below 4 μ m thickness, allowing for an efficient particle acceleration.

The main importance of our work resides in the successful operation of a compact, cost-effective tool for future studies related to laser-ion acceleration. In that sense, the data obtained from plain foil targets constitute a benchmark test; their consistency with former experiments shows that all components of our setup are well under control. A major laser upgrade is presently under preparation, comprising an increase in pulse energy to 500 mJ (pre-compression, about twice the present value). Following the dotted trend line of Figure 8 we assume that this should give rise to protons of 3 MeV maximum energy at least; former experiments even achieved 4-5 MeV [15, 20, 21]. At the same time the total number of protons (of the order 10^6 - 10^7 /msr) may increase to 10^7 - 10^8 /msr as suggested by previous publications under similar conditions [8, 9, 13, 18, 21, 30].

Laser-based proton accelerators are still at an early stage of evolution and major developments are necessary to exploit their potential as compact and stable particle sources. These comprise a continuous operation during several hours at high shot rate, an optimized laser-plasma energy transfer giving rise to increased particle energies, and a control of the particle spectra and beam divergence. A sophisticated target design (possibly with micro- or nano-structures) will be a key technique for all these aspects [39–41]. Our compact setup can be a valuable tool for abundant tests of such targets and the evaluation of their performance in comparison to reference materials (like the flat foils reported here) and particle-in-cell simulations. As such, it allows for studies of the underlying physics of laser-plasma interactions as well as technical developments related to laser-based proton beams.

Acknowledgments

The authors highly appreciate the collaboration of Radosys (Budapest) which provided CR-39 detector material, etching bath, and readout equipment. This project has been funded by Centro para el Desarrollo Tecnológico Industrial (CDTI, Spain) within the INNPRONTA program, grant no. IPT-20111027, by EUROSTARS project E9113, and by the Spanish Ministry for Economy and Competitiveness within the Retos-Colaboración 2015 initiative, ref. RTC-2015-3278-1.

References

- [1] H. Daido, M. Nishiuchi, and A.S. Pirozhkov, *Review of laser-driven ion sources and their applications*, *Rep. Prog. Phys.* **75** (2012) 056401.
- [2] A. Macchi, M. Borghesi, and M. Passoni, *Ion acceleration by superintense laser-plasma interaction*, *Rev. Mod. Phys.* **85** (2013) 751-793.
- [3] K.W.D. Ledingham, P.R. Bolton, N. Shikazono, and C.-M. Ma, *Towards laser driven hadron cancer radiotherapy: A review of progress*, *Applied Sciences* **4** (2014) 402-443.
- [4] S.D. Kraft et al., *Dose-dependent biological damage of tumour cells by laser-accelerated proton beams*, *New Journal of Physics* **12** (2010) 085003.

- [5] A. Yogo et al., *Application of laser-accelerated protons to the demonstration of DNA double-strand breaks in human cancer cells*, *Appl. Phys. Lett.* **94** (2009) 181502.
- [6] S. Fritzler et al., *Proton beams generated with high-intensity lasers: Applications to medical isotope production*, *Appl. Phys. Lett.* **83** (2003) 3039-3041.
- [7] H. Kishimura et al., *Enhanced generation of fast protons from a polymer-coated metal foil by a femtosecond intense laser field*, *Appl. Phys. Lett.* **85** (2004) 2736-2738.
- [8] S. Nakamura et al., *Real-time optimization of proton production by intense short-pulse laser with time-of-flight measurement*, *Jap. J. Appl. Phys.* **45** (2006) L913.
- [9] M. Nishiuchi et al., *The laser proton acceleration in the strong charge separation regime*, *Phys. Lett. A* **357** (2006) 339-344.
- [10] A. Yogo et al., *Laser prepulse dependency of proton-energy distributions in ultraintense laser-foil interactions with an online time-of-flight technique*, *Physics of Plasmas* **14** (2007) 043104.
- [11] A.P.L. Robinson et al., *Spectral modification of laser-accelerated proton beams by self-generated magnetic fields*, *New Journal of Physics* **11** (2009) 083018.
- [12] K. Nemoto et al., *Laser-triggered ion acceleration and table top isotope production*, *Appl. Phys. Lett.* **78** (2001) 595-597.
- [13] K. Lee et al., *Generation of intense proton beams from plastic targets irradiated by an ultraintense laser pulse*, *Phys. Rev. E* **78** (2008) 056403.
- [14] A. Yogo et al., *Laser ion acceleration via control of the near-critical density target*, *Phys. Rev. E* **77** (2008) 016401.
- [15] K. Lee et al., *Dominant front-side acceleration of energetic proton beams from plastic targets irradiated by an ultraintense laser pulse*, *Physics of Plasmas* **18** (2011) 013101.
- [16] S. Okihara et al., *Energetic proton generation in a thin plastic foil irradiated by intense femtosecond lasers*, *J. Nucl. Sci. Technol.* **39** (2002) 1-5.
- [17] P. McKenna et al., *Characterization of multiterawatt laser-solid interactions for proton acceleration*, *Rev. Sci. Instrum.* **73** (2002) 4176-4184.
- [18] I. Spencer et al., *Experimental study of proton emission from 60-fs, 200-mJ high-repetition-rate tabletop-laser pulses interacting with solid targets*, *Phys. Rev. E* **67** (2003) 046402.
- [19] M. Kaluza et al., *Influence of the laser prepulse on proton acceleration in thin-foil experiments*, *Phys. Rev. Lett.* **93** (2004) 045003.
- [20] T. Ceccotti et al., *Proton acceleration with high-intensity ultrahigh-contrast laser pulses*, *Phys. Rev. Lett.* **99** (2007) 185002.
- [21] D. Neely et al., *Enhanced proton beams from ultrathin targets driven by high contrast laser pulses*, *Appl. Phys. Lett.* **89** (2006) 021502.
- [22] S. Steinke et al., *Efficient ion acceleration by collective laser-driven electron dynamics with ultra-thin foil targets*, *Laser and Particle Beams* **28** (2010) 215-221.
- [23] M. Roth and M. Schollmeier, *Ion acceleration—Target Normal Sheath Acceleration*, *CERN Yellow Reports* **1** (2016) 231.
- [24] D. Strickland and G. Mourou, *Compression of amplified chirped optical pulses*, *Optics Communications* **56** (1985) 219-221.

- [25] A. Yogo et al., *Insertable pulse cleaning module with a saturable absorber pair and a compensating amplifier for high-intensity ultrashort-pulse lasers*, *Opt. Express* **22** (2014) 2060-2069.
- [26] A. Trisorio et al., *Self-referenced spectral interferometry for ultrashort infrared pulse characterization*, *Opt. Lett.* **14** (2012) 2892-2894.
- [27] F. Lindau, *Laser-driven particle acceleration—Experimental investigations*, Ph.D. thesis, *Lund Reports in Atomic Physics* **LRAP-378** (2007), ISBN 978-91-628-7167-3.
- [28] M. Seimetz et al., *Calibration and performance tests of detectors for laser-accelerated protons*, *IEEE Trans. Nucl. Sci.* **62** (2015) 3216-3224.
- [29] F. Nürnberg et al., *Radiochromic film imaging spectroscopy of laser-accelerated proton beams*, *Rev. Sci. Instrum.* **80** (2009) 033301.
- [30] Y. Oishi et al., *Dependence on laser intensity and pulse duration in proton acceleration by irradiation of ultrashort laser pulses on a Cu foil target*, *Physics of Plasmas* **12** (2005) 073102.
- [31] M. Nishiuchi et al., *Focusing and spectral enhancement of a repetition-rated, laser-driven, divergent multi-MeV proton beam using permanent quadrupole magnets*, *Appl. Phys. Lett.* **94** (2009) 061107.
- [32] P. Antici et al., *Energetic protons generated by ultrahigh contrast laser pulses interacting with ultrathin targets*, *Physics of Plasmas* **14** (2007) 030701.
- [33] J.S. Green et al., *Enhanced proton flux in the MeV range by defocused laser irradiation*, *New Journal of Physics* **12** (2010) 085012.
- [34] K. Zeil et al., *The scaling of proton energies in ultrashort pulse laser plasma acceleration*, *New Journal of Physics* **12** (2010) 045015.
- [35] M. Nishiuchi et al., *Efficient production of a collimated MeV proton beam from a polyimide target driven by an intense femtosecond laser pulse*, *Physics of Plasmas* **15** (2008) 053104.
- [36] A. Macchi, A. Sgattoni, S. Sinigardi, M. Borghesi, and M. Passoni, *Advanced strategies for ion acceleration using high-power lasers*, *Plasma Phys. Control. Fusion* **55** (2013) 124020.
- [37] A. Macchi, *Laser-driven ion acceleration*, in: P. Bolton, K. Parodi, J. Schreiber (eds.), *Applications of laser-driven particle acceleration*, CRC press, 2017 (to be published).
- [38] J. Fuchs et al., *Laser-driven proton scaling laws and new paths towards energy increase*, *Nature Physics* **2** (2006) 48-54.
- [39] H. Schwöerer et al., *Laser-plasma acceleration of quasi-monoenergetic protons from microstructured targets*, *Nature* **439** (2006) 445-448.
- [40] D. Margarone et al., *Laser-driven proton acceleration enhancement by nanostructured foils*, *Phys. Rev. Lett.* **109** (2012) 234801.
- [41] K.A. Flippo et al., *Increased efficiency of short-pulse laser-generated proton beams from novel flat-top cone targets*, *Physics of Plasmas* **15** (2008) 056709.